Hindawi Publishing Corporation
Journal of Nanomaterials
Volume 2014, Article ID 576082, 7 pages
http://dx.doi.org/10.1155/2014/576082

Research Article

Shape-Controlled Generation of Gold Nanoparticles Assisted by Dual-Molecules: The Development of Hydrogen Peroxide and Oxidase-Based Biosensors

Chifang Peng, Xiaohui Duan, Zhengjun Xie, and Chunli Liu

State Key Laboratory of Food Science and Technology, School of Food Science and Technology, Jiangnan University, Wuxi 214122, China

Correspondence should be addressed to Chifang Peng; pcf@jiangnan.edu.cn

Received 29 June 2014; Accepted 5 September 2014; Published 13 October 2014

Academic Editor: Marinella Striccoli

With the assist of dual-molecules, 2-(N-morpholino)ethanesulfonic acid (MES) and sodium citrate, gold nanoparticles (GNPs) with different shapes can be generated in the H_2O_2-mediated reduction of chloroauric acid. This one-pot reaction can be employed to sensitively detect H_2O_2, probe substrates or enzymes in oxidase-based reactions as well as prepare branched GNPs controllably. By the "naked eye," 20 μM H_2O_2, 0.1 μM glucose, and 0.26 U/mL catalase could be differentiated, respectively. By spectrophotometer, the detected limits of H_2O_2, glucose, and catalase were 1.0 μM, 0.01 μM, and 0.03 U/mL, respectively, and the detection linear ranges for them were 5.0–400 μM, 0.01–0.3 mM, and 0.03–0.78 U/mL, respectively. The proposed "dual-molecules assist" strategy probably paves a new way for the fabrication of nanosensors based on the growth of anisotropic metal nanoparticles, and the developed catalase sensor can probably be utilized to fabricate ultrasensitive ELISA methods for various analytes.

1. Introduction

Gold nanoparticles (GNPs) possess distinct physical and chemical attributes that make them excellent scaffolds for the fabrication of novel chemical and biological sensors [1]. Interestingly, some unique sensors based on GNP enlargement of GNP seeds have been developed, such as colorimetric sensors for enzymes and substrates in biocatalyzed reactions [2] and light scattering signal enhancer in scanometric immunoassay [3]. Recently, the generation of GNPs has also been utilized to develop some novel sensors, such as chemiluminescence sensor based on DNA structure catalyzing the formation of GNPs [4] that produce gold nanoshells for detecting hydrogen peroxide scavenging activity [5] and liquid crystal biosensors based on enzymatic deposition of GNPs [6].

The accurate and rapid determination of H_2O_2 is of practical importance due to its application in food, pharmaceutical, clinical, industrial, and environmental analysis [5, 7]; H_2O_2 is generally acknowledged to be an oxidative agent. However, it has been reported to be able to reduce $HAuCl_4$ to synthesize AuNPs in a broad pH range [8]. Recently, de la Rica et al. described a visual H_2O_2 sensor, based on which an ultrasensitive enzyme-linked immunosorbent assay (ELISA) for prostate specific antigen was developed. The above visual H_2O_2 sensor was based on H_2O_2-mediated generation of GNPs in MES buffer. An abrupt change in the solution color from red to blue happened when the concentration of H_2O_2 was under a cut-off value [9, 10]. Nevertheless, this novel method cannot be utilized to quantitatively detect targets. It also should be noted that gold precursors have to be prepared first by using MES as a reducing agent in this method [11]. In this step, unstable GNPs aggregates are easily produced [12], which will bring about difficulty and inconvenience in practical applications. Since the stability of GNPs is affected by many factors, such as reducing agents, surfactants [13], the above H_2O_2 sensor based on GNPs generation probably can be improved by adjusting these additives.

Herein, we utilized dual-molecules, sodium citrate (Na_3Cit) and MES, to control the generation of GNPs in the H_2O_2-mediated reduction of $AuCl_4^-$. It was found that this H_2O_2-mediated GNPs generation can be utilized to qualitatively detect H_2O_2 and prepare branched GNPs. Based on the above discovery, a sensitive and simple H_2O_2 sensor by the naked eye was developed. Catalase and glucose were

taken as examples to show the applications of this H_2O_2 sensor.

2. Experimental Section

Reagents. The reagents, $HAuCl_4$, sodium citrate, MES, and catalase (C1345), were purchased from Sigma-Aldrich. Glucose and GOD (G109029) were purchased from Aladdin Reagent Company (Shanghai). High-purity water (Milli-Q water) was used throughout the experiments. All other reagents are of analytical grade unless otherwise stated.

Effects of Buffers on the Generation of GNP Solutions. 3 μL of $HAuCl_4$ (30 mM), 6 μL of Na_3Cit (80 mM) were mixed thoroughly with 91 μL MES (2.0 mM, pH 6.5), phosphate buffer (2.0 mM, pH 6.5) or tris-(hydroxymethyl)aminoethane buffer (Tris, 2.0 mM, pH 6.5) buffer (2.0 mM, pH = 6.5), were mixed thoroughly; then 100 μL of H_2O_2 was added and incubated at ambient temperature for 10 min. Na_3Cit or MES was replaced by the same volume of ultrapurified water in the above reaction to investigate their effects. In addition, varied concentrations of Na_3Cit (20, 40, 80, and 120 mM) were compared in the above reaction system with $HAuCl_4$, MES, and H_2O_2.

Characterization of GNPs. Absorbance spectra were measured by microplate spectrophotometer (Bio-Tek PowerWave XS). Size distribution and zeta potential of GNPs were measured by Zetasizer Nano ZS (Malvern) after the GNPs were produced within 15 min. Transmission electron microscopy (TEM) images were obtained using JEOL JEM-2100 operating at an acceleration voltage of 200 kV.

Detection of H_2O_2. In a representative procedure, 3 μL of $HAuCl_4$ (20 mM), 6 μL of Na_3Cit (40 mM), and 91 μL of MES buffer (2.0 mM, pH = 6.5) were mixed thoroughly; then 100 μL of H_2O_2 was added. After incubating at ambient temperature for 10 min, absorbance spectra were recorded.

Detection of Catalase. 50 μL of catalase (0–40 nM) and 50 μL of H_2O_2 (400 μM) were mixed and incubated at ambient temperature for 20 min. Then the reaction solutions were added into the mixture of 3 μL of $HAuCl_4$ (20 mM), 6 μL of Na_3Cit (40 mM), and 91 μL of MES (2.0 mM, pH 6.5). After incubating for another 10 min, absorbance spectra were recorded.

Detection of Glucose. 50 μL of GOx (50 μg/mL) and 50 μL of glucose (0–30 mM) were mixed first and incubated at ambient temperature for 20 min. Then the reaction solutions were added into the mixture of 3 μL of $HAuCl_4$ (20 mM), 6 μL of Na_3Cit (40 mM), and 91 μL of MES (2.0 mM, pH 6.5). After incubating for another 10 min, absorbance spectra were recorded.

3. Results and Discussion

3.1. Development of H_2O_2 Sensor. Usually, MES can reduce $HAuCl_4$ and produce a blue color [12]. After H_2O_2 was added to the mixture of MES and $HAuCl_4$, only high concentration of H_2O_2 (200 μM) could be differentiated by the naked eye (Figure 1(a)). The absorbance intensity of the GNPs solution increased with the increasing concentration of H_2O_2 in a very narrow range of 100–400 μM (Figure 1(b)). Thus, the reaction was substoichiometric and not sensitive for sensing H_2O_2 mainly due to the formed unstable aggregated gold nanostructures (See Figure S1 at Supplementary Material available online at http://dx.doi.org/10.1155/2014/576082). As expected, sodium citrate (Na_3Cit) can act as stabilizer to improve

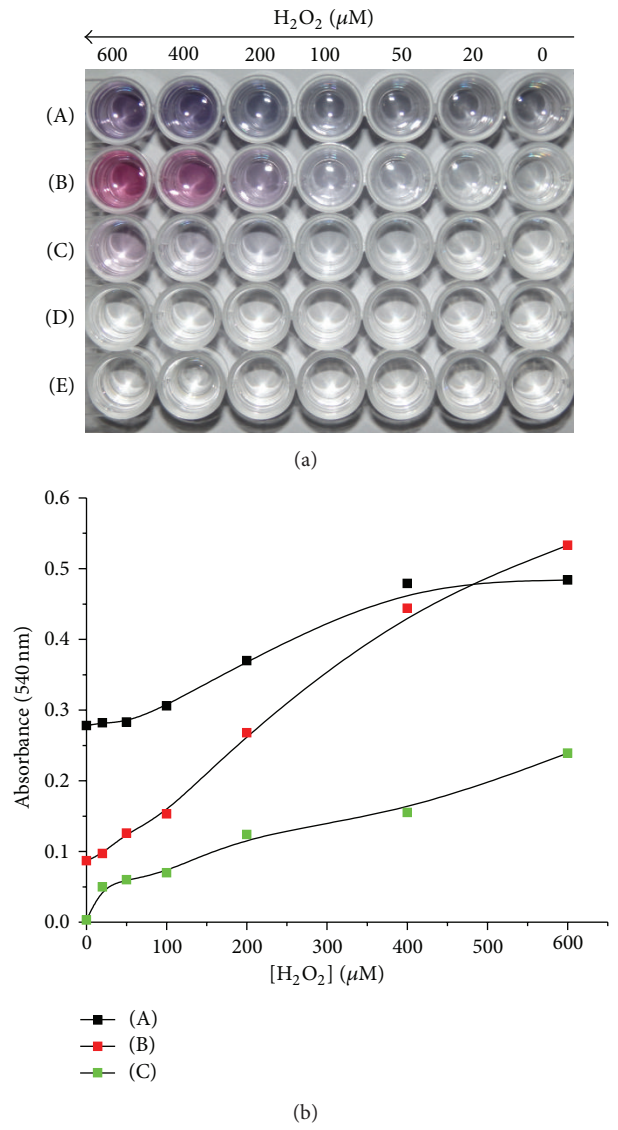

Figure 1: GNP solutions generated in different buffers. (a) Photograph showing the reaction solution. (b) Absorbance values (540 nm) of GNP solutions as a function of H_2O_2 concentration. Reaction condition: (A) 0.45 mM $HAuCl_4$ and 1.0 mM MES (pH = 6.5); (B) 0.45 mM $HAuCl_4$, 2.4 mM sodium citrate, and 1.0 mM MES (pH = 6.5); (C) 0.45 mM $HAuCl_4$, 2.4 mM sodium citrate, and water; (D) 0.45 mM $HAuCl_4$, 2.4 mM sodium citrate, and 1.0 mM PB (pH = 6.5); (E) 0.45 mM $HAuCl_4$, 2.4 mM sodium citrate, and 1.0 mM Tris (pH = 6.5).

the sensing performance against H_2O_2. With the addition of Na_3Cit (20 mM) into MES-$AuCl_4^-$ solution, the MES-Na_3Cit-$AuCl_4^-$ reaction solution without H_2O_2 became colorless. The result shows that Na_3Cit can act as an "inhibitor" of the reduction of $AuCl_4^-$ by MES to some extent. As a result, 20 μM H_2O_2 could be differentiated by the naked eye (Figure 1(a)). More importantly, the color of GNPs deepened gradually as the concentration of H_2O_2 increased in the range of 0–600 μM. This result was consistent with the nearly linear plot of the absorbance values of the produced GNPs solutions versus H_2O_2 concentrations in the range from 0 μM to 600 μM (Figure 1(b)). Interestingly, Na_3Cit also can assist the H_2O_2-mediated reduction of $AuCl_4^-$ although the reduction is very weak (Figures 1(a)-1(b)). H_2O_2 cannot reduce $AuCl_4^-$ into GNPs in other common buffers containing Na_3Cit, such as phosphate buffer or tris(hydroxymethyl)aminomethane buffer (Figure 1(a)). The above comparison suggests that MES and Na_3Cit together can work synergistically, leading to a more specific reduction of $AuCl_4^-$ by H_2O_2 than only MES.

Na_3Cit can stabilize the GNPs generated to some extent because the produced GNPs in the $AuCl_4^-$/MES/H_2O_2 reaction became smaller after adding 0.4 mM Na_3Cit. When 400 μM H_2O_2 was added into $HAuCl_4$-MES-Na_3Cit solution, the average hydrodynamic diameter of produced GNPs was 49 nm, while the bigger GNPs (mean hydrodynamic diameter = 108 nm) assembled by smaller GNPs were obtained in the absence of Na_3Cit (Figure S1). With the added Na_3Cit being increased from 40 mM to 120 mM, the produced GNPs showed almost the same color and the plots of the absorbance intensity versus H_2O_2 concentration highly overlapped (Figure S2). But after decreasing the concentration of Na_3Cit to 10 mM, the absorbance intensity corresponding to 400 μM H_2O_2 became occasionally lower than that corresponding to 200 μM. This result is due to the fact that the produced high concentration of GNPs solution does not have enough Na_3Cit and easily forms aggregate. Since the pH value and concentration of MES probably change the reduction ability of MES, we varied the pH value and concentration of MES to choose the best pH and concentration of MES. The best pH value was found to be 6.5 (Figure S3). The MES concentration also affects the performance of the above H_2O_2 sensor probably due to the changed ratio of MES to Na_3Cit (Figure S4).

In a representative condition, GNPs solutions with different tonality could be obtained depending on the concentration of H_2O_2 (Figure 2(a)). Light blue solutions corresponding to lower concentration of H_2O_2 (20–100 μM) were obtained, and purple to wine red solutions corresponding to higher concentration of H_2O_2 (200–600 μM) were produced. As a result, 20 μM H_2O_2 can be detected by the naked eye. Colorimetric assay showed that the maximum absorbance values increased and the GNPs surface plasmon resonance (SPR) peak blue-shifted from 560 nm to 540 nm as the concentration of H_2O_2 increased (Figure 2(b)). The blueshift of SPR peak in this system was opposite to the redshift usually observed in seed-mediated gold enlargement systems [2, 5]. After the concentration of H_2O_2 decreased to 100 μM, obviously broadening of the SPR peaks was observed. This abrupt change of SPR peaks was consistent with the change of red color to light blue color.

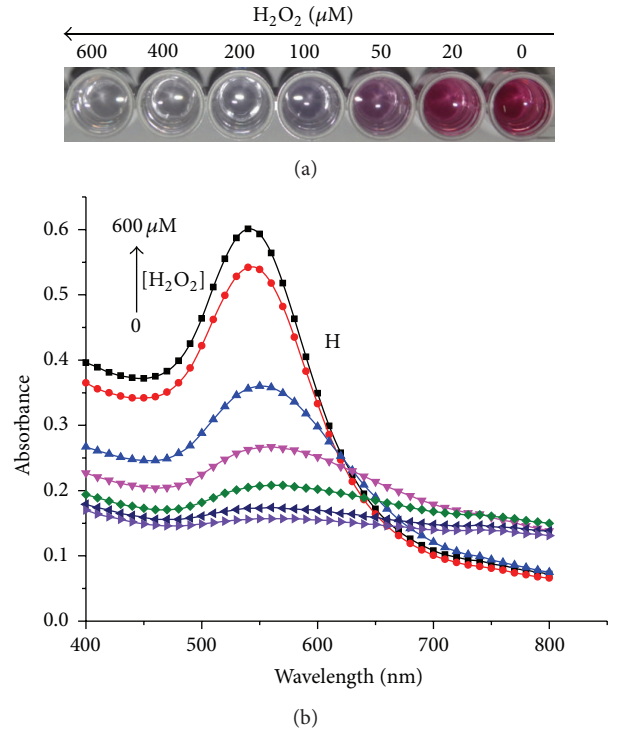

Figure 2: Generation of GNP solutions with different colors depends on the concentration of H_2O_2. (a) Photograph showing the generation of nanoparticle solutions with different colors and intensities after 10 min. (b) Absorbance spectra of GNPs generated with different concentration of H_2O_2. From bottom to up: 0, 50, 100, 200, 400, and 600 μM.

Because MES (1.0 mM) was excessive to $AuCl_4^-$ (0.45 mM) while H_2O_2 (0–400 μM) was insufficient to reduce all the $AuCl_4^-$, the AuNPs generation probably changed after H_2O_2 was consumed completely. However, it was found that the AuNPs generation reached a plateau after 10 minutes and then the developed color changed very slowly. After the color developing for 60 min, 25 μM H_2O_2 still can be differentiated by the naked eye (Figure 3(a)) and 5 μM H_2O_2 by spectrophotometry (Figure 3(b)). These results demonstrate that this one-pot reaction has a wide window for analysis of H_2O_2, which can facilitate practical applications. When H_2O_2 was detected by a spectrophotometer, a linear range of 2–400 μM (R^2 = 99.6%) was obtained and the detection limit (S/N = 3) is evaluated as 0.5 μM (Figure 4). The sensitivity of the developed method here is higher or comparable with that of some other nanoparticle-based colorimetric H_2O_2 sensors [7, 14, 15].

To further understand the interesting property of this visual H_2O_2 sensor, we observed the shapes of the GNPs reduced by the different concentration of H_2O_2. Branched GNPs comprising branched nanocrystals with about 10 nm dimension were found by the reduction of 100 μM H_2O_2 (Figures 5(a)–5(e)). GNP dimers comprising 20–25 nm branches can be found by the reduction of 400 μM H_2O_2 (Figure 5(f)), while dispersed quasi-spherical GNPs in the dimension of 30–40 nm can be found by the reduction of

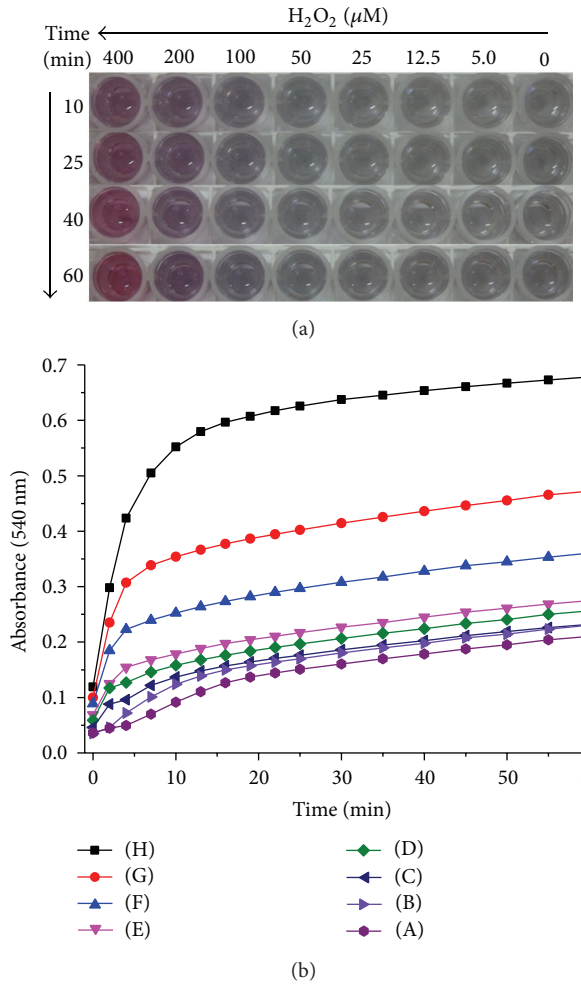

FIGURE 3: H_2O_2 (0–400 μM) reduction of GNPs over time: (A) 0 μM, (B) 5 μM, (C) 12.5 μM, (D) 25 μM, (E) 50 μM, (F) 100 μM, (G) 200 μM, and (H) 400 μM H_2O_2.

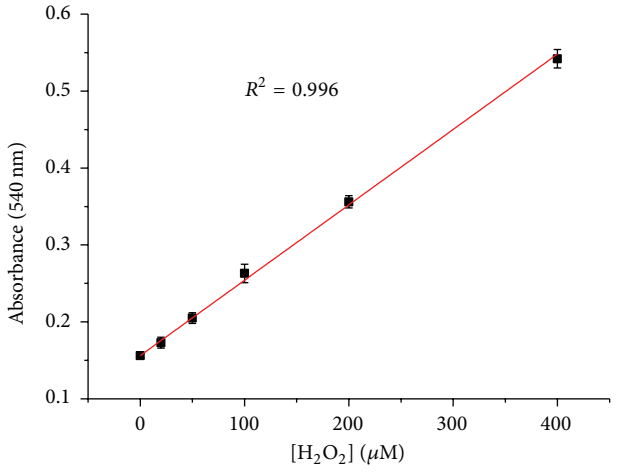

FIGURE 4: Calibration curve for quantitative detection of H_2O_2. H_2O_2 reduction of GNPs kept for 10 min. The error bars represent standard derivations.

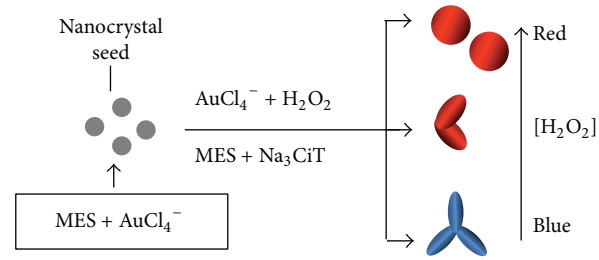

SCHEME 1: Cartoon of the generation of different shapes of GNPs.

600 μM H_2O_2 (Figure 5(g)). This finding is probably useful in controllable synthesis of branched GNPs, which is very useful for the fabrication of nanosensors, multiple-terminal devices, and so forth [16].

The entirely different shapes of GNPs generated in the presence of varied concentrations of H_2O_2 suggest that two processes at least will happen in this MES-Na_3Cit-$AuCl_4^-$-H_2O_2 reaction (Scheme 1). One process involves the reduction of $AulCl_4^-$ by MES. Since, with the addition of Na_3Cit and in the absence of H_2O_2, MES still produced weak reduction of $AuCl_4^-$, MES can act like an "initiator" (Figure 1(b)). MES also functions like other zwitterionic molecules under certain conditions since many Good's buffers can serve as shape-directing agents in synthesis of branched gold nanocrystals [16]. Another process involves the reduction of $AulCl_4^-$ by MES, which mainly depends on the reduction of $AuCl_4^-$ by H_2O_2. With the addition of increased H_2O_2, the enlargement of gold nanoparticles gradually overwhelms the generation of the branched gold nanocrystals.

Detection of Glucose. Numerous oxidases can produce H_2O_2 upon the oxidation of the respective substrates by O_2. It suggests that this $AuCl_4^-$/MES/Na_3Cit system can probably be employed as an effective tool for the visual sensing of oxidases and their substrates. We have applied this system to detect glucose by using glucose oxidase (GOD) and glucose/O_2 as H_2O_2 producing system. Figure 6(a) shows the visual detection results of glucose in this reaction system. The solution color deepened gradually as the glucose concentration was increased. Light blue solution was produced corresponding to 0.03–0.1 mM glucose while purple solution was produced corresponding to 0.3–1.0 mM glucose. After glucose concentration increased to above 3.0 mM, the produced solutions changed to bright red wine. This color change can be distinguished clearly by the naked eye. This sensitivity is comparable with the method reported recently but shows more distinguishable and controllable color development model [17]. Figure 6(b) showed that the absorbance intensity of reaction solutions increased gradually as the glucose concentration increased. The detection limit of 0.01 mM glucose (S/N = 3) and linear range from 0.01 to 0.3 mM were obtained by spectrophotometry (Figure 6(b)). The sensitivity is higher than or comparable with that of the colorimetric methods recently reported [7, 14, 17, 18].

Detection of Catalase. Catalase is very important enzyme in protecting the cell from oxidative damage by reactive

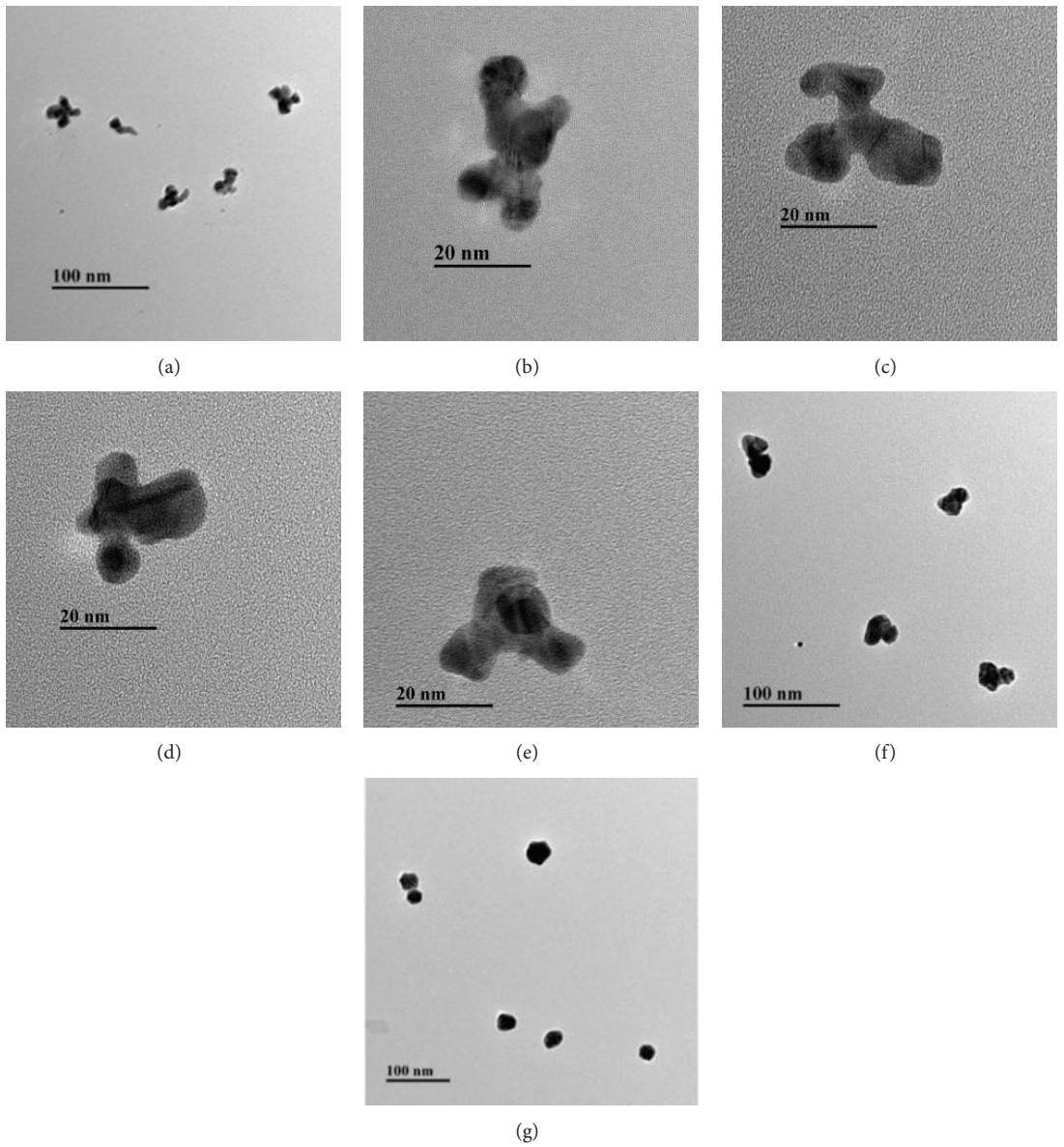

Figure 5: TEM images of GNPs generated with varied H_2O_2 concentrations: (a–e) 100 μM H_2O_2, (f) 400 μM H_2O_2, and (g) 600 μM H_2O_2.

oxygen species. Catalase is also a key indicator of mastitis disease in milk [19, 20]. Thus, facile detection catalase will be useful in many fields. Since catalase can decompose H_2O_2 efficiently, coupling this decomposition with the above $AuCl_4^-$/MES/Na_3Cit reaction can probably be utilized to probe the activity of catalase. As expected, the performance adverse to that of the above H_2O_2 detection was found (Figure 7(a)). As the concentration of catalase increased from 0.03 U/mL to 21.0 U/mL, different solution colors from wine red and purple to light blue were demonstrated. By the naked eye, 0.3 U/mL of catalase can be clearly distinguished. In addition, the detection limit of 0.026 U/mL catalase (S/N = 3) can be achieved by spectrophotometry (Figure 7(b)). The sensitivity of the "naked eye" or colorimetric methods developed here is higher than the surface plasmon resonance (SPR) method [20] and amperometric biosensor reported recently [19] or comparable with that of some expensive commercial available kits for catalase detection.

4. Conclusions

In conclusion, gold nanoparticles (GNPs) with different shapes can be generated in the reduction of $HAuCl_4$ by varied concentration of H_2O_2 with the assist of dual-molecules, 2-(N-morpholino)ethanesulfonic acid (MES) and sodium citrate. This simple $AuCl_4^-$/MES/Na_3Cit/H_2O_2 reaction system can also be employed to sensitively detect H_2O_2 by "naked eye" and has been applied to probe substrate or enzyme in oxidase-based reactions. This interesting H_2O_2 sensor is ascribed to a proposed "dual-molecules assist" mechanism.

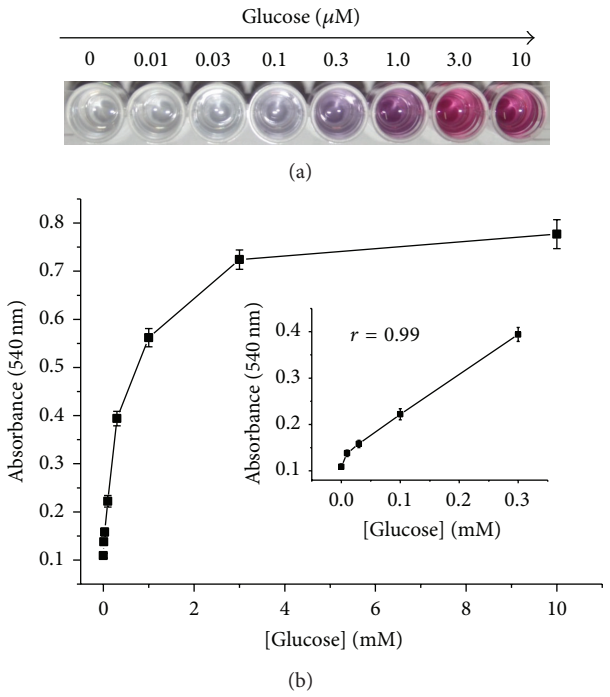

Figure 6: Generation of nanoparticle solutions with different colors depends on the concentration of glucose. (a) Photograph showing the generation of GNP solutions with different colors and intensities. (b) Plots of absorbance values of GNP solutions against the concentration of glucose. Inset: linear relationship between absorbance values and glucose concentrations.

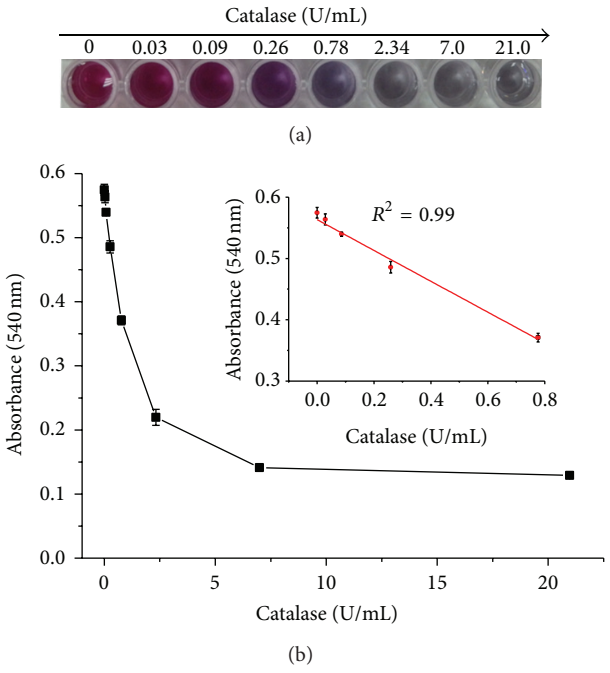

Figure 7: Generation of nanoparticle solutions with different colors depends on the concentration of catalase. (a) Photograph showing the generation of GNP solutions with different colors and intensities. (b) Plots of absorbance values of GNP solutions against the concentration of catalase. Inset: linear relationship between absorbance values and catalase concentrations.

Since many other Good's buffers besides MES can reduce $AuCl_4^-$ and many other molecules besides sodium citrate function as stabilizers in the synthesis of GNPs, a great deal of combination can be explored to optimize the performance of these H_2O_2 and oxidase-based sensors. The developed catalase sensor can probably be utilized to fabricate ultrasensitive ELISA methods for various analytes, which is now being studied by our group. Additionally, branched anisotropic GNPs can be synthetized via this "dual-molecules assist" strategy.

Conflict of Interests

The authors declare that there is no conflict of interests regarding the publication of this paper.

Acknowledgments

This work was supported by the National Natural Science Foundation of China (31371767), the 12th Five Years Key Programs (2012BAK08B01), the Natural Science Foundation of Jiangsu Province (BK20141108), and the Research Program of State Key Laboratory of Food Science and Technology, Jiangnan University (SKLF-ZZA-201202).

References

[1] L. Xu, H. Kuang, C. Xu, W. Ma, L. Wang, and N. A. Kotov, "Regiospecific plasmonic assemblies for *in Situ* Raman spectroscopy in live cells," *Journal of the American Chemical Society*, vol. 134, no. 3, pp. 1699–1709, 2012.

[2] L. Wang, L. Xu, H. Kuang, C. Xu, and N. A. Kotov, "Dynamic nanoparticle assemblies," *Accounts of Chemical Research*, vol. 45, no. 11, pp. 1916–1926, 2012.

[3] J. He, Y. Liu, T. C. Hood, P. Zhang, J. Gong, and Z. Nie, "Asymmetric organic/metal(oxide) hybrid nanoparticles: synthesis and applications," *Nanoscale*, vol. 5, no. 12, pp. 5151–5166, 2013.

[4] D. Liu, Z. Wang, and X. Jiang, "Gold nanoparticles for the colorimetric and fluorescent detection of ions and small organic molecules," *Nanoscale*, vol. 3, no. 4, pp. 1421–1433, 2011.

[5] Y. Zhou, S. Wang, K. Zhang, and X. Jiang, "Visual detection of copper(II) by azide- and alkyne-functionalized gold nanoparticles using click chemistry," *Angewandte Chemie International Edition*, vol. 47, no. 39, pp. 7454–7456, 2008.

[6] H. Jans and Q. Huo, "Gold nanoparticle-enabled biological and chemical detection and analysis," *Chemical Society Reviews*, vol. 41, no. 7, pp. 2849–2866, 2012.

[7] H. Kuang, W. Chen, W. Yan et al., "Crown ether assembly of gold nanoparticles: melamine sensor," *Biosensors and Bioelectronics*, vol. 26, no. 5, pp. 2032–2037, 2011.

[8] Y. Xiao, V. Pavlov, S. Levine, T. Niazov, G. Markovitch, and I. Willner, "Catalytic growth of Au nanoparticles by NAD(P)H cofactors: optical sensors for $NAD(P)^+$-dependent biocatalyzed transformations," *Angewandte Chemie*, vol. 43, no. 34, pp. 4519–4522, 2004.

[9] M. Zayats, R. Baron, I. Popov, and I. Willner, "Biocatalytic growth of Au nanoparticles: from mechanistic aspects to biosensors design," *Nano Letters*, vol. 5, no. 1, pp. 21–25, 2005.

[10] D. Kim, W. L. Daniel, and C. A. Mirkin, "Microarray-based multiplexed scanometric immunoassay for protein cancer markers

using gold nanoparticle probes," *Analytical Chemistry*, vol. 81, no. 21, pp. 9183–9187, 2009.

[11] S. Cai, K. Lao, C. Lau, and J. Lu, ""Turn-on' chemiluminescence sensor for the highly selective and ultrasensitive detection of Hg2+ ions based on interstrand cooperative coordination and catalytic formation of gold nanoparticles," *Analytical Chemistry*, vol. 83, no. 24, pp. 9702–9708, 2011.

[12] H. Li, X. Ma, J. Dong, and W. Qian, "Development of methodology based on the formation process of gold nanoshells for detecting hydrogen peroxide scavenging activity," *Analytical Chemistry*, vol. 81, no. 21, pp. 8916–8922, 2009.

[13] S. Liao, Y. Qiao, W. Han et al., "Acetylcholinesterase liquid crystal biosensor based on modulated growth of gold nanoparticles for amplified detection of acetylcholine and inhibitor," *Analytical Chemistry*, vol. 84, no. 1, pp. 45–49, 2012.

[14] Y. Jv, B. Li, and R. Cao, "Positively-charged gold nanoparticles as peroxidiase mimic and their application in hydrogen peroxide and glucose detection," *Chemical Communications*, vol. 46, no. 42, pp. 8017–8019, 2010.

[15] X. Liu, H. Xu, H. Xia, and D. Wang, "Rapid seeded growth of monodisperse, quasi-spherical, citrate-stabilized gold nanoparticles via H_2O_2 reduction," *Langmuir*, vol. 28, no. 38, pp. 13720–13726, 2012.

[16] R. De La Rica and M. M. Stevens, "Plasmonic ELISA for the ultrasensitive detection of disease biomarkers with the naked eye," *Nature Nanotechnology*, vol. 7, no. 12, pp. 821–824, 2012.

[17] P. Gobbo, M. J. Biondi, J. J. Feld, and M. S. Workentin, "Arresting the time-dependent H_2O_2 mediated synthesis of gold nanoparticles for analytical detection and preparative chemistry," *Journal of Materials Chemistry B*, vol. 1, no. 33, pp. 4048–4051, 2013.

[18] R. de la Rica and M. M. Stevens, "Plasmonic ELISA for the detection of analytes at ultralow concentrations with the naked eye," *Nature Protocols*, vol. 8, no. 9, pp. 1759–1764, 2013.

[19] C. Engelbrekt, K. H. Sørensen, J. Zhang, A. C. Welinder, P. S. Jensen, and J. Ulstrup, "Green synthesis of gold nanoparticles with starch-glucose and application in bioelectrochemistry," *Journal of Materials Chemistry*, vol. 19, no. 42, pp. 7839–7847, 2009.

[20] M. Grzelczak, J. Pérez-Juste, P. Mulvaney, and L. M. Liz-Marzán, "Shape control in gold nanoparticle synthesis," *Chemical Society Reviews*, vol. 37, no. 9, pp. 1783–1791, 2008.